sustainability

MDPI

Article

Variation of Ground Surface Freezing/Thawing Index in China under the CMIP6 Warming Scenarios

Xianglong Li [1], Ze Zhang [1,*], Andrey Melnikov [2], Mingyi Zhang [3], Doudou Jin [4] and Jinbang Zhai [4]

[1] School of Civil Engineering, Institute of Cold Regions Science and Engineering, Permafrost Institute, Northeast Forestry University, Harbin 150040, China
[2] Melnikov Permafrost Institute, Siberian Branch, Russian Academy of Science, 677010 Yakutsk, Russia
[3] State Key Laboratory of Frozen Soil Engineering, Northwest Institute of Eco-Environment and Resources, Chinese Academy of Sciences, Lanzhou 730000, China
[4] School of Transportation, Northeast Forestry University, Harbin 150040, China
* Correspondence: zez@nefu.edu.cn

Abstract: As an important parameter in permafrost research, the annual ground surface freezing/thawing index is widely used in the variation of permafrost. In addition, it is also an important indicator in climatology, providing a large amount of theoretical basis for the assessment of climate change. Based on the ground surface temperature data recorded at 707 meteorological stations from 1960 to 2020, the ground surface freezing/thawing index in China were calculated. The results showed that over the past six decades, the thawing index has shown an upward trend, whereas the freezing index has shown a downward trend, and the trend is stronger around 2000. The results of the R/S-based analysis indicate that the freezing/thawing index will remain on a decreasing/increasing trend for some time to come. Based on the five warming scenarios published by Coupled Model Intercomparison Project Phase 6 (CMIP6), the spatial–temporal variation characteristics of the ground surface freezing/thawing index in China during 2020–2100 was simulated. It was found that under SSP3-7.0 and SSP5-8.5 scenarios, the freezing/thawing index may be 0 °C-days in 2080 and 2070, respectively, which may imply that the ground surface freezing process in some regions of China may disappear.

Keywords: China; ground surface freezing/thawing index; CMIP6; SSP; warming scenarios

check for updates

Citation: Li, X.; Zhang, Z.; Melnikov, A.; Zhang, M.; Jin, D.; Zhai, J. Variation of Ground Surface Freezing/Thawing Index in China under the CMIP6 Warming Scenarios. *Sustainability* **2022**, *14*, 14458. https://doi.org/10.3390/su142114458

Academic Editor: Mohammad Valipour

Received: 4 October 2022
Accepted: 2 November 2022
Published: 3 November 2022

Publisher's Note: MDPI stays neutral with regard to jurisdictional claims in published maps and institutional affiliations.

Copyright: © 2022 by the authors. Licensee MDPI, Basel, Switzerland. This article is an open access article distributed under the terms and conditions of the Creative Commons Attribution (CC BY) license (https://creativecommons.org/licenses/by/4.0/).

1. Introduction

Permafrost refers to a thermal state of the ground with a temperature of 0 °C or below for two years or more [1]. Permafrost is extremely vulnerable to temperature changes, and some regions are experiencing permafrost degradation and disappearance as the air temperature rises [2–4]. The degradation and loss of permafrost can lead to the degradation of surface vegetation cover, resulting in a marked increase in ecosystem vulnerability [5–8]. In addition, the thawing of permafrost induces geological hazards, such as frost heave and thaw subsidence, which have important impacts on cold-zone projects and greatly increase the cost of construction and maintenance [9–13].

To understand the changes in permafrost under global warming, interannual and interdecadal changes in permafrost need to be analyzed [14]. Because permafrost is highly susceptible to climate change, it is relatively difficult to establish direct monitoring of permafrost, and there are few methods to quantify its storage and spatial distribution [15]. The freezing/thawing index is considered to be an effective indicator for studying permafrost changes and is used not only to estimate the distribution of permafrost [16], but also to assess the active layer thickness and freezing depth of seasonal permafrost and permafrost [17], such as in the calculation of Stefan's equation and the n-factor, where the freezing/thawing index is a very important parameter [18–20]. In addition, the freezing/thawing index is also a very important factor in the study of climatic meteorology. By

comparing the freezing/thawing index of a certain year, the trend of climate change in the region can be known [21], which can provide reference for the policy formulation of the corresponding management measures.

The freezing/thawing index can be divided into two types: one is the air freezing/thawing index, and the other is the ground surface freezing/thawing index. The air freezing/thawing index refers to the accumulated value of mean daily air temperature below/higher than 0 at 1.5 m above the surface, whereas the ground surface freezing/thawing index refers to the accumulated value of temperature below/higher than 0 at 0 m above the ground surface [22,23]. There is a large number of literature studies on the air freezing/thawing index [24,25]. However, most of the current studies on the ground surface freezing/thawing index in China are focused on the Qinghai–Tibet Plateau and the northeastern part of China [26,27]; in addition to these permafrost regions, there are many regions with seasonal permafrost distribution and the transition area between permafrost areas, and the calculation of the freezing/thawing index for the entire Chinese region is important for our understanding of various permafrost and ground surface process changes. In terms of freezing/thawing index prediction, Peng [28] used CMIP5 data to predict the spatial and temporal variation of the freezing/thawing index in the Arctic. Solang [29] used CMIP5 data to simulate and predict the freezing/thawing index in Qian tang Nature Reserve in China; compared with CMIP5, CMIP6 has improved and developed in terms of resolution and experimental design, and CMIP6 has designed more experiments and simulated more complex physical processes, while correcting the long-standing model bias in CMIP5 [30]. Therefore, it is necessary to use more accurate data (CMIP6) to simulate the ground surface freeze-thaw index, the results of which provide a more accurate basis for the assessment of permafrost, climate, and greenhouse gases.

In this study, the annual ground surface freezing/thawing index was calculated for the period 1960–2020 in China using ground surface temperature data, and the temporal variation characteristics of the freezing/thawing index were analyzed and discussed using statistical methods. In addition, the freezing/thawing index is simulated for the period 2020–2100 by combining the five warming scenario data of CMIP6. The research in this study will further enhance our understanding of hydrological, ecological, and environmental changes in China under global warming, and the results of the study can provide a reference for decision making by relevant authorities.

2. Data and Methods

2.1. Data

The ground surface temperature data are from the China Meteorological Administration (CMA, http://data.cma.cn/dataService/cdcindex/datacode/A.0013.0001/show_value/normal.html (accessed on 18 July 2021)); this link gives us access to daily scale ground temperature data. There are 845 meteorological stations in China, and the data recorded by these stations are not exactly the same; some stations recorded data only until the 1990s, and some stations recorded data from the 1970s [31,32], so the data recorded by meteorological stations with continuous time between 1960 and 2020 are used in this study for the calculation of the annual ground surface freezing/thawing index, and 707 meteorological stations were selected after screening. The specific details of the screening and data processing are: (1) if one day of data was missing in one month, the average of the previous day and the day after was selected instead; (2) if data are missing for more than two days in a month, but not more than five days, the average data for the year before and after the missing time period are selected instead; (3) if more than five days of data were missing in a month, the weather station is discarded [20]. The distribution of 707 weather stations is shown in Figure 1.

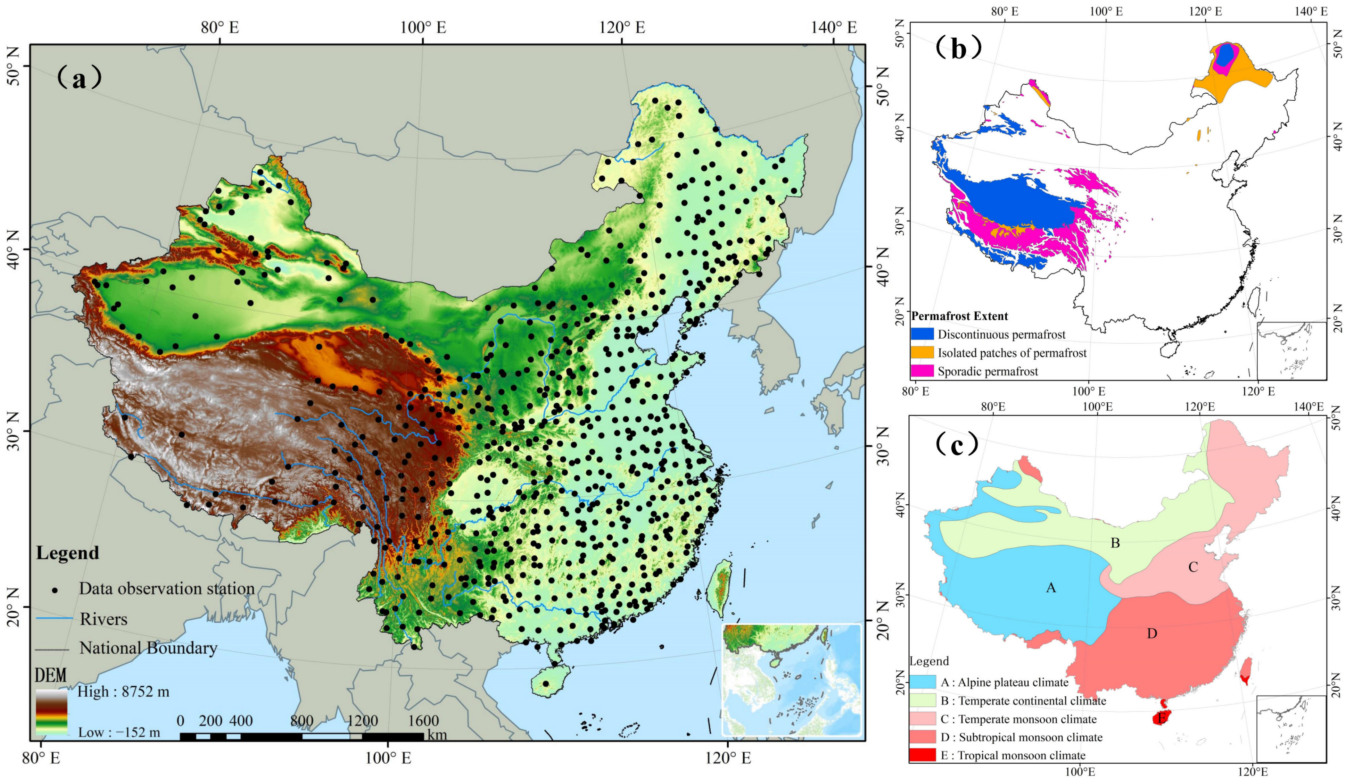


Figure 1. Overview of the study area; (**a**) distribution of meteorological stations and DEM of the study area; (**b**) different permafrost distributions of the study area, data available from http://nsidc.org/data (accessed on 18 July 2021); (**c**) climate type of the study area.

Climate scenario data are published by the CMIP6 (https://esgf-node.llnl.gov/search/cmip6/ (accessed on 18 July 2021)). The climate scenarios are the result of a combination of projections due to differences in the socio-economic development, climate change scenarios, and control of greenhouse gases. These five scenarios are: very high greenhouse gas (GHG) emissions (the fifth scenario: SSP5-8.5), high GHG emissions (the fourth scenario: SSP3-7.0), moderate GHG emissions (the third scenario: SSP2-4.5), and low GHG emissions (the first and second scenarios: SSP1-1.9 and SSP1-2.6). These five scenarios correspond to five possible future global surface warming patterns, and the warming patterns are shown in Figure 2.

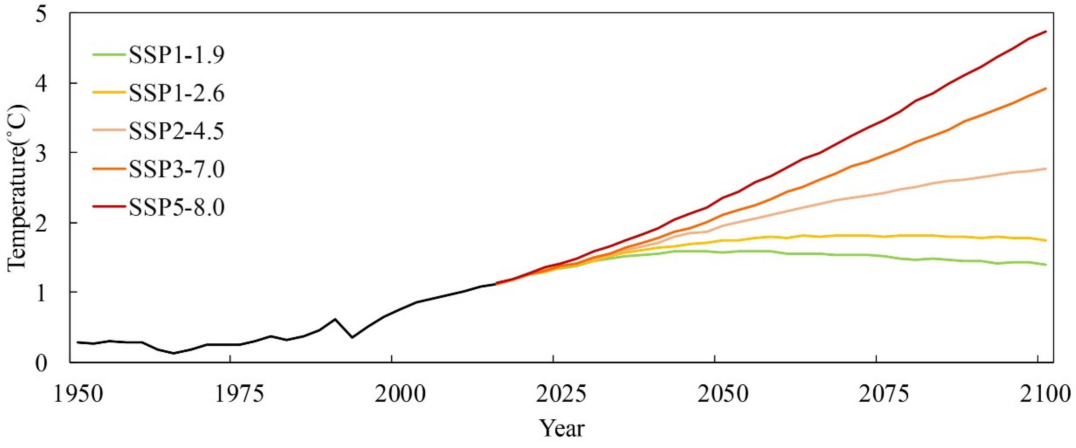


Figure 2. Global surface temperature changes relative to 1850–1900; the data are from the CMIP6 on five warming scenarios.

2.2. Methods

The freezing index is the cumulative value of the mean daily ground surface temperature below 0 in a year, and the thawing index is the cumulative value of the mean daily ground surface temperature above 0 in a year [33,34]. In this study, in order to ensure that the same freezing/thawing period temperature data is used in the calculation of the freezing/thawing index, we have specified that the freezing index is calculated from 1 July to 30 June of the following year, and the thawing index is calculated from 1 January to 31 December of the same year. They can be calculated by the expressions (1) and (2):

$$\mathrm{FI}_S = \sum_{i=1}^{M_f} \left|\overline{T}_i\right| \cdot D_i, \overline{T}_i < 0\ ^\circ\mathrm{C} \quad (1)$$

$$\mathrm{TI}_S = \sum_{i=1}^{M_t} \left|\overline{T}_i\right| \cdot D_i, \overline{T}_i > 0\ ^\circ\mathrm{C} \quad (2)$$

where s represents the ground surface, $\overline{T}_i$ is the average ground surface temperature of month i, FI_S is the annual ground surface freezing index, and TI_S is the annual ground surface thawing index. M_f and M_t are the months in which the monthly average ground surface temperature is above/below 0 °C, and D_i is the number of days.

A total of seven model data were selected through completeness screening of the different model scenario data (Table 1). Because of the inconsistent and low spatial resolution of the data, all pattern data in this study were downscaled to 0.25° × 0.25° by a bilinear interpolation method [35]. Multi-model averaging can significantly improve the simulation results compared to single-model, as has been demonstrated in a number of studies [36–38]; therefore, the subsequent simulations and predictions in this study are the results of multi-model averaging. The specific process for calculating the future freezing/thawing index using CMIP6 data is shown in Figure 3.

Table 1. Information on the different models of CMIP6.

No.	Model Name	Country	Horizontal Resolution	References
1	BCC-CSM2-MR	China	1.1° × 1.1°	Wu [39]
2	CAS-ESM2-0	China	1.4° × 1.4°	Zhang [40]
3	CESM2	USA	1.3° × 0.9°	Lauritzen [41]
4	CESM2-WACCM	USA	1.3° × 0.9°	Liu [42]
5	E3SM-1-1	USA	1.0° × ~1.0°	Golaz [43]
6	E3SM-1-1-ECA	USA	1.0° × ~1.0°	Golaz [43]
7	MRI-ESM2-0	Japan	1.1° × 1.1°	Yukimoto [44]

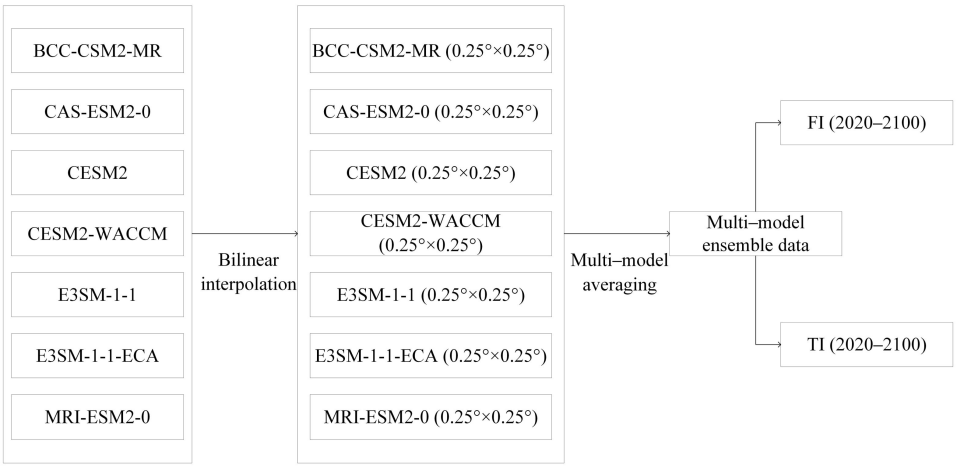


Figure 3. Process for calculating the freezing/thawing index in China over the period 2020–2100.

Trend detection is one of the common means of detecting climate change in the currently available literature [45]. In this study, two trend detection methods were selected. The first method is the M-K test method: the test method of M-K is the non-parametric test method. The non-parametric test method is also called the non-distribution test. The advantage is that the known data do not need to follow certain distribution rules (e.g., Gaussian distribution) when participating in the calculation, and it is not affected by individual outliers [46,47]. The second method is rescaled range (R/S) analysis, which can distinguish a random sequence from a non-random sequence, and it can also perform the exploration of long-term memory processes in nonlinear systems. The R/S analysis method is usually used as the fractal characteristics and future trend analysis of time series data, and was applied to the analysis of the geological and meteorological data time series [48–50]. R/S analysis is a nonlinear time series analysis method which has advantages in the persistence and anti-persistence of time series changes; its calculation can be evaluated by the Hurst [51,52]. The calculation results can be divided into the following three cases: (1) the past change trend and the future change trend are independent of each other (Hurst = 0.5). (2) The trend of present change is opposite to the future (0 < Hurst < 0.5). (3) The present change trend is the same as the future (0.5 < Hurst < 1). In particular, it is important to point out that the stronger the calculation results are close to 0 and 1, the stronger the anti-persistence and persistence.

3. Results

3.1. The Variation of Ground Surface Freezing/Thawing Index from 1960 to 2020

The spatially continuous thawing index distribution was obtained by spatial interpolation of known meteorological station data over the period 1960–2020 [53], which identifies the cumulative value of annual positive temperature and reflects the warmth of different regions in China (Figure 4a). From south to north, the thawing index shows a significant decreasing trend, which reflects the relationship between the thawing index and latitude, with a lower thawing index in regions of higher latitudes. With the increase of altitude, the thawing index showed a downward trend. Figure 4b is the spatial variation trend of the thawing index. The thawing index in most regions increases by about (5.3–10.1) °C-days per year. Especially in the southwest, northwest, southern, and northeastern regions, the thawing index increases by more than 10 °C-days per year. In particular, in some permafrost regions, such as the Qinghai–Tibet Plateau and Greater Hinggan Mountains, the thawing index also increases significantly, reflecting the fact that the ground surface freezing/thawing cycle is reducing under a warming climate.

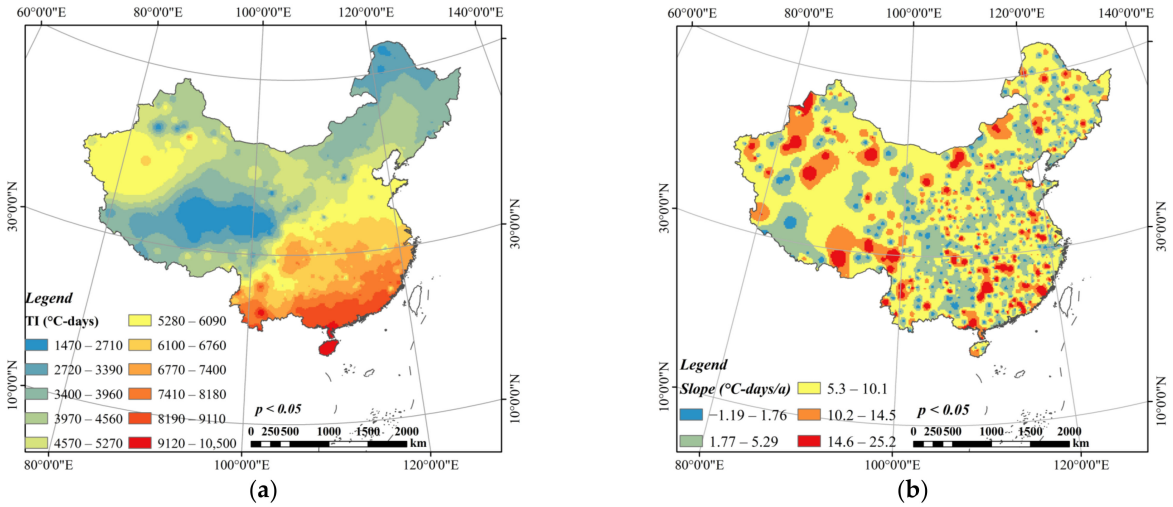


Figure 4. Ground surface thawing index (TI) (**a**) and the trends of thawing index (**b**) in China from 1960 to 2020.

The annual ground surface thawing index shows a fluctuating increase between 1960 and 2020 (Figure 5). Furthermore, by examining the time series of the thawing index, it was found that the thawing index trend changed in 1998 (M–K test method). Before 1998, the thawing index increased by 4.74 °C-days per year. After 1998, the thawing index increased by 6.74 °C-days per year.

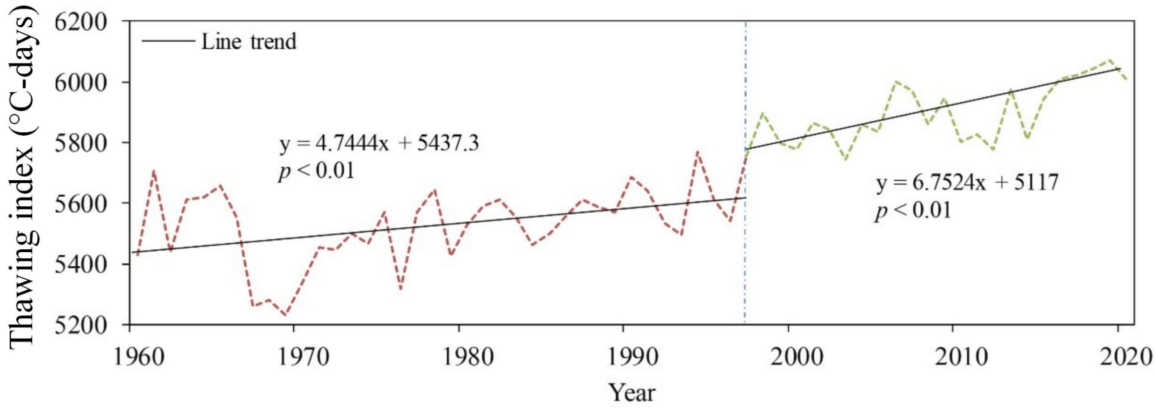


Figure 5. Temporal variation of annual ground surface thawing index in China from 1960 to 2020.

The spatially continuous freezing index distribution was obtained by spatial interpolation of known meteorological station data over the period from 1960–2020 [53]. Figure 6a shows the spatial distribution of the freezing index in China. It can be seen that the freezing index is higher in regions of high latitude and high altitude, and decreases with decreasing latitude and altitude. In some areas of permafrost, the freezing index can reach as high as 3300 °C-days. Figure 6b shows the variation trend of the freezing index. The freezing index in most areas of China is decreasing. As the latitude increases, the downward trend becomes more obvious. Especially in the northeast of China, Inner Mongolia, and the northwest of China, the downward trend exceeds 27 °C-days per year.

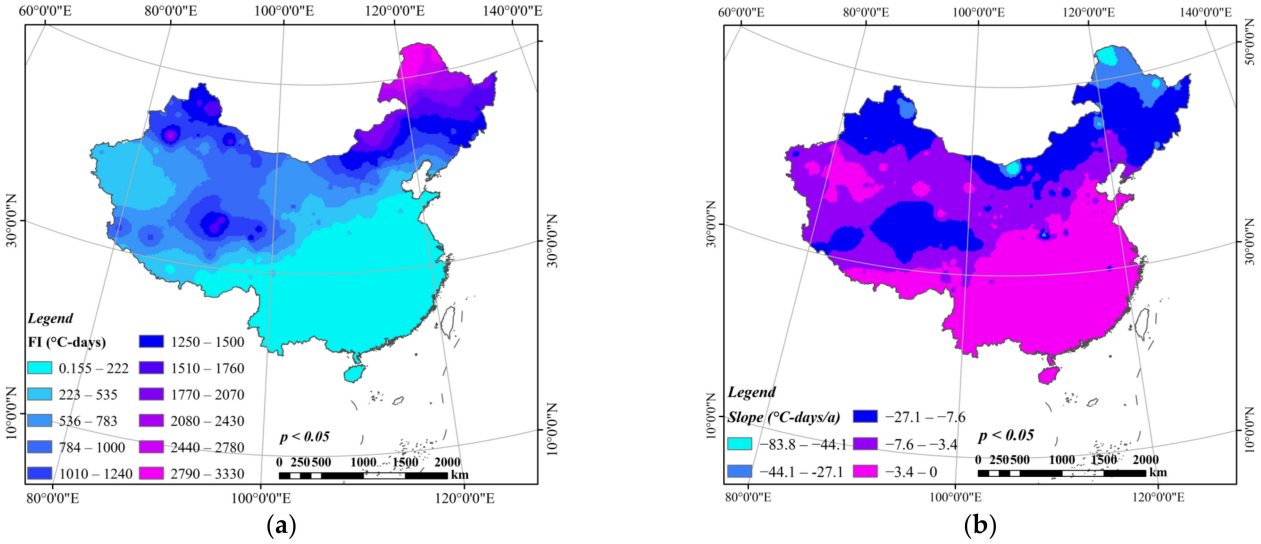


Figure 6. Ground surface freezing index (**a**) and the trends of freezing (**b**) index in China from 1960 to 2020.

During 1960–2020, the freezing index shows fluctuating decreasing changes (Figure 7), and by detecting and analyzing these time series data, it was found that the freezing index trend changed in 2004 (M–K test), and the downward trend of the freezing index before and after 2004 was significantly different. Before 2004, the freezing index decreased relatively

slowly, with a rate of −2.02 °C-days per year, and then after 2004, the freezing index decreased significantly faster, with a rate of −11.94 °C-days per year.

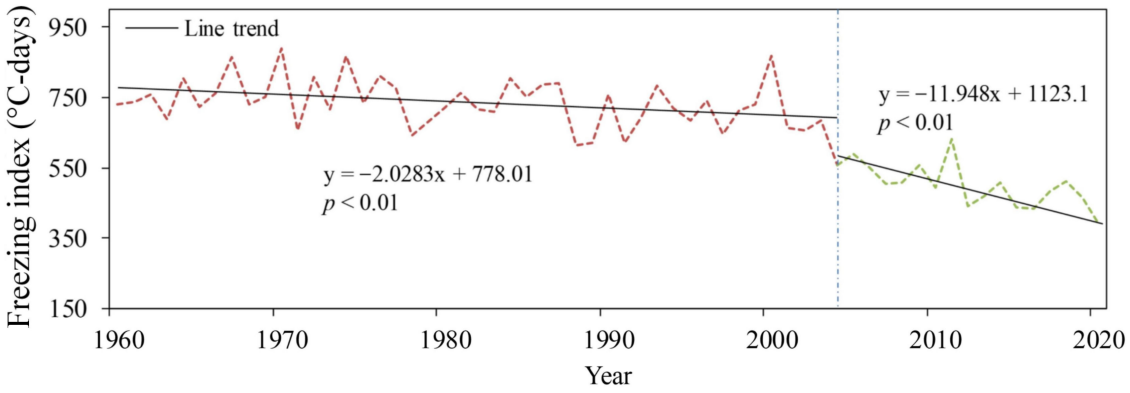


Figure 7. Temporal variation of annual ground surface freezing index in China from 1960 to 2020.

As can be seen from Figure 8, there is a significant positive correlation between the annual mean ground surface temperature and annual thawing index, with a correlation coefficient of 0.94. The fitted graph shows that the annual surface freezing index decreases with increasing annual ground surface temperature, and the fitted correlation is very significant, and the correlation coefficient is −0.91. The slope is the value of the annual ground surface freezing/thawing index with the annual mean ground surface temperature, which can be calculated by the least square method. The thawing index increases by 477.42 °C-days and the freezing index decreases by 251.96 °C-days with temperature increases by 1 °C. All the results of the above calculations were statistically significant.

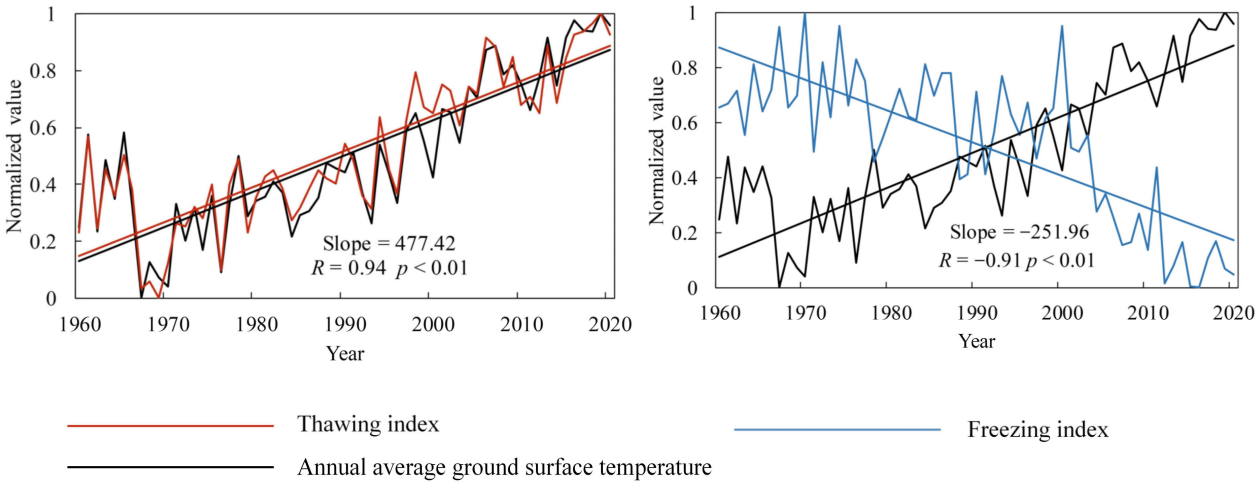


Figure 8. Variation of ground surface freezing/thawing index with ground surface temperature in China from 1960 to 2020. Note: All variables are normalized.

Figure 9 shows the regression scatter fitted line equation, and Table 2 shows the value of different parameters calculated for the freezing/thawing index Hurst index. The Hurst index is all greater than 0.80, indicating that there is an obvious Hurst phenomenon (i.e., there is a relatively good continuation of the trend). The past trend of the freezing/thawing index will continue in the future, which means that the thawing index will maintain the current upward trend, whereas the freezing index will maintain the current upward trend; these results are statistically significant.

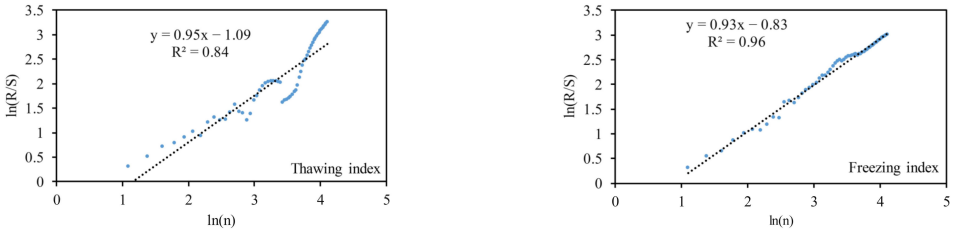


Figure 9. R/S analysis on thawing index and freezing index in China from 1960 to 2020.

Table 2. Hurst value of thawing index and freezing in China from 1960 to 2020.

Area	Hurst	R^2	*p*
Thawing index	0.95	0.84	0.00 **
Freezing index	0.93	0.96	0.00 **

Note: ** denotes significance at $p < 0.01$.

3.2. The Variation of Ground Surface Freezing/Thawing Index from 2020 to 2100

Based on the five warming scenarios data of CMIP6, the spatial–temporal variation characteristics of the freezing/thawing index in China from 2020 to 2100 are discussed. As can be seen from Figure 10a, in the SSP1-1.9 and SSP1-2.6 warming scenarios, the thawing index will remain within 6500 °C-days. In the SSP2-4.5 and SSP3-7.0 warming scenarios, the thawing index of China will reach 6700 °C-days and 7300 °C-days by 2100. In the SSP5-8.5 (worst) warming scenario, the thawing index in China will exceed 7500 °C-days by 2100. As can be seen from Figure 10b, the future trend of the freezing index in China is quite obvious. In the SSP1-1.9 and SSP1-2.6 warming scenarios, the freezing index showed a downward trend, and after the middle of the century, the freezing index showed a certain upward trend. In the SSP2-4.5 warming scenario, the freezing index will decrease faster before the middle of the century, and then the freezing index will slow down. In the SSP3-7.0 and SSP5-8.5 warming scenarios, the freezing index will decrease to 0 °C-days in 2080 and 2070, respectively, and this would mean that the freezing process in some regions of China may disappear.

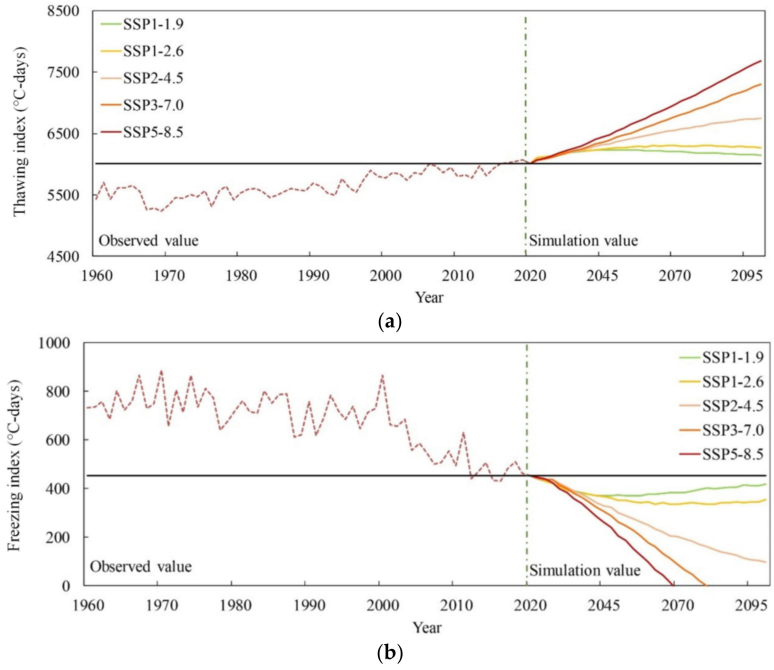


Figure 10. Simulation results of thawing index (**a**) and freezing index (**b**) under different warming models in China (observed values (dotted lines), simulated values (solid lines)).

Based on the above research, the spatial variation characteristics of the thawing index were analyzed (Figure 11). It can be seen that the thawing index has an obvious upward trend in the past 60 years. In addition, the spatial characteristics of the thawing index changes, according to the warming patterns under five scenarios, were mapped (2020–2100, plotted every 20 years). It can be seen that under the first and second warming scenarios, the thawing index in the study area increased by a small range. Under the SSP1-1.9 and SSP1-2.6 warming scenarios, the thawing index of the whole region increased significantly. Under the SSP5-8.5 scenario, most of the areas will have a thawing index of more than 5000 °C-days, except for the Tibetan Plateau and some areas in northeast China.

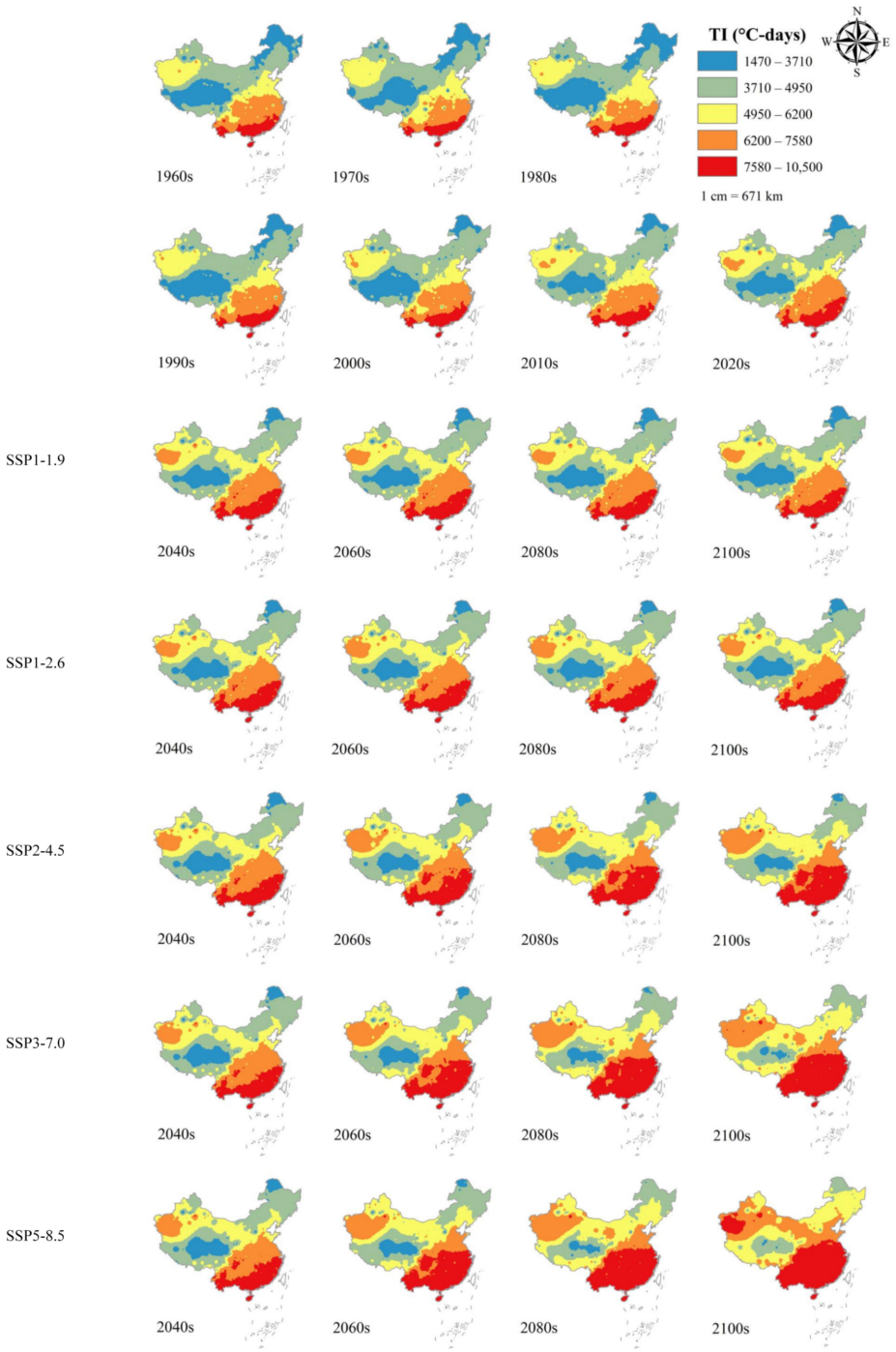


Figure 11. Spatial variation of the thawing index in China (observed values (1960–2020), simulated values (2020–2100)).

The spatial variation characteristics of the freezing index were analyzed (Figure 12). From 1960 to 1980, the freezing index in the Qinghai–Tibet Plateau and northeast China had a significant change. From 1980 to 2000, except for the Qinghai–Tibet Plateau, the freezing index of China had little change. Since 2000, the freezing index in China has been declining obviously. Similarly, the spatial variation characteristics of the freezing index in the next 80 years were simulated by analyzing the surface temperature and five warming scenarios. In the SSP1-1.9 and SSP1-2.6 warming scenarios, the freezing index changes little. Under the SSP2-4.5, SSP3-7.0, and SSP5-8.5 warming scenarios, most of the areas' freezing index will drop below 300 °C-days in around 2080, except for the Tibetan Plateau and northeast China. Under the SSP5-8.5 warming scenario, the freezing index in China will approach 0 °C-days by 2100.

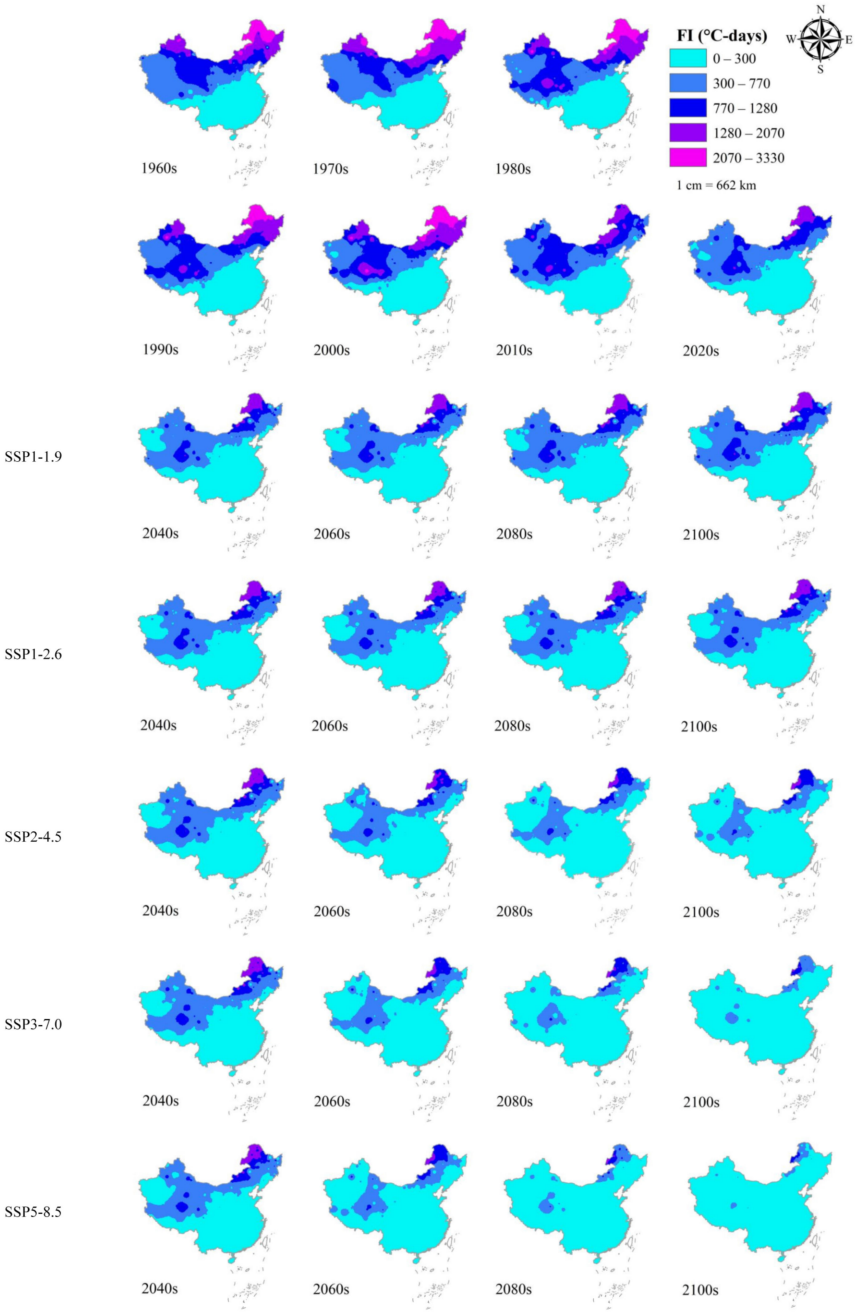


Figure 12. Spatial variation of the freezing index in China (observed values (1960–2020), simulated values (2020–2100)).

4. Discussion

The ground surface freezing/thawing index is an assessment of cold (warmth), which measures the ground surface–atmosphere heat condition and indicates the depth and intensity of the freeze–thaw action [24,25]. In the above-mentioned study, the past and future changes of the ground surface freezing/thawing index were analyzed. In this subsection, we discuss how the freezing/thawing index changes in permafrost regions and how it changes in different climatic zones.

4.1. Freezing and Thawing Variations Associated with Permafrost

The variation of the freezing and thawing index in our permafrost and non-permafrost zones is compared, and the variation of the freezing and thawing index for the observation period, as well as for the five scenarios, is quantified (Figure 13). The results of the thawing index indicate that the rate of the thawing index change in permafrost regions, where human activity is relatively low, is close to that of the non-permafrost regions. A comparison of the observed values with the change in the thawing index for the different scenarios revealed that the change in the thawing index over the period of the observations was close to that of the SSP2-4.5 scenario. When the warming scenario is SSP5-8.0, the slope of the thaw index will be 18.5 °C-day/a and 21.1 °C-day/a for the permafrost and non-permafrost regions, respectively, and the change of the thawing index in this scenario will be more than twice the change in the observed thawing index. Comparing the change of the freezing index between permafrost and non-permafrost regions, the change of the freezing index is much higher in permafrost regions than in non-permafrost regions, due to the lower thawing index in non-permafrost regions; when, in a given year, the freezing index becomes 0 °C-day/a, it will no longer decrease. It is also evident from the change of the freezing index in permafrost regions that the permafrost may be undergoing an active degradation process; in particular, when the warming scenario is SSP5-8.0, the slope of the freezing index will be nearly twice the observed value.

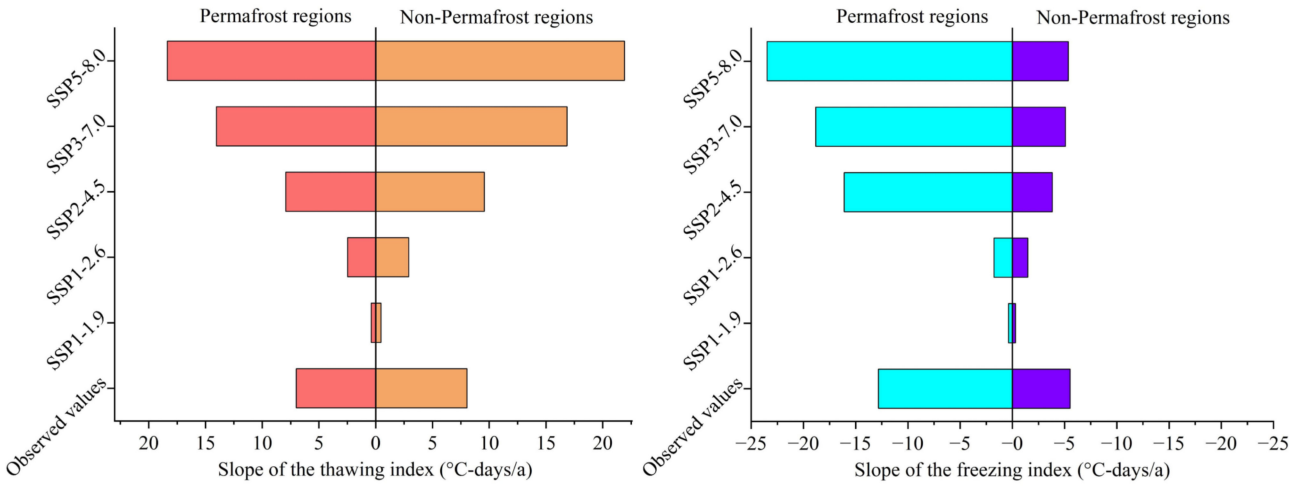


Figure 13. Variations of freezing/thawing index in permafrost and non-permafrost regions in China. Note: the statistical time range of the observed values are from 1960 to 2020; the statistical time range for the five warming scenarios are from 2020 to 2100.

In order to observe the variation of the freezing/thawing index for different types of permafrost, we calculated the slope of the freeze–thaw index for the observed values (1960–2020), SS1-1.9 (2020–2100), SSP1-2.6 (2020–2100), SS2-4.5 (2020–2100, SSP3-7.0 (2020–2100), and SSP5-8.0 (2020–2100) (Figure 14). It can be seen that the variation of the freezing/thawing index is lower than observed value for all three permafrost types in the SSP1-1.9 and SSP1-2.6 scenarios, and in particular, the slope of the variation of the freezing/thawing index is lower than 0.5 in the SSP1-1.9 scenario, indicating that SSP1-1.9 is a very favorable scenario for sustainable development. In terms of the slope of the thawing

index, the observed thawing index increases at a rate close to the SSP2-4.5 scenario for all three permafrost types at present, whereas in terms of the slope of change in the freezing index, only at discontinuous permafrost do the observed values of the freezing index change close to the SSP2-4.5, the other two being lower than the SSP2-4.5 scenario. Secondly, by comparing the variation of the freezing/thawing index in the different permafrost type regions, it can be seen that the slope of the change in the freezing/thawing index from high to low is discontinuous permafrost, sporadic permafrost, and isolated patches of permafrost, with both the freezing and thawing indexes reflecting this characteristic, which may indicate that the rate of permafrost degradation is higher in the discontinuous permafrost region than in the sporadic permafrost and isolated patches of permafrost.

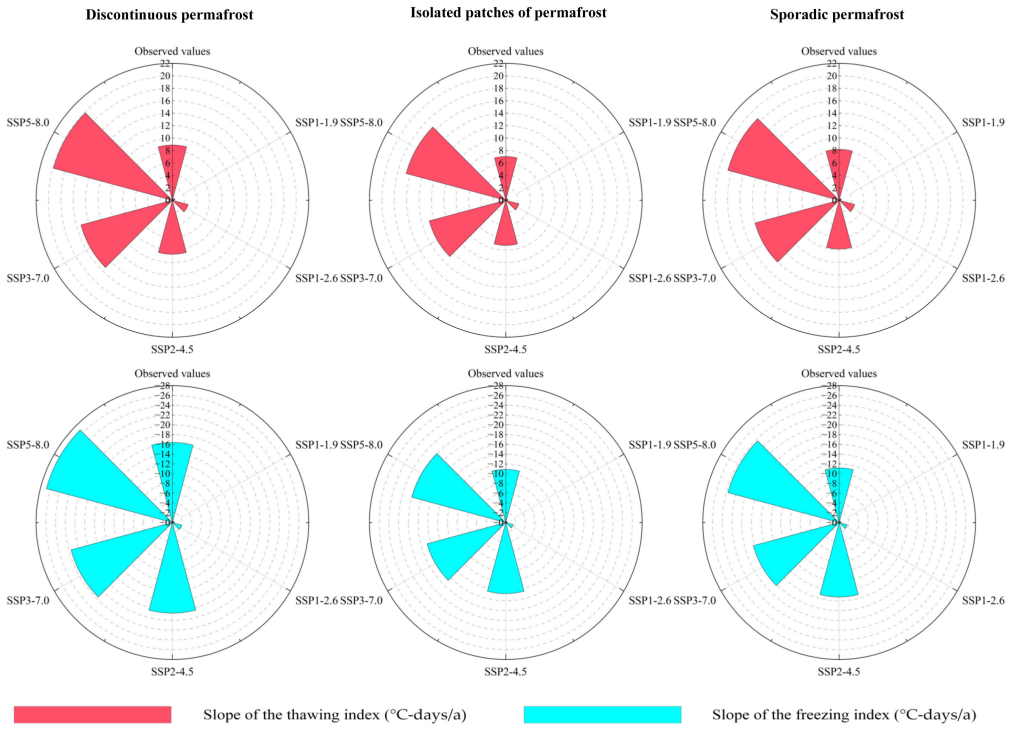


Figure 14. Comparison of the variations of the freezing/thawing index under different permafrost types in China. Note: the statistical time range of the observed values are from 1960 to 2020; the statistical time range for the five warming scenarios are from 2020 to 2100.

4.2. Variations of Ground Freezing/Thawing Index in Different Climatic Zones

In order to make a more accurate analysis of the future freezing/thawing index in China, the study area was divided into five sub-regions according to different climate types (Figure 1c). These five sub regions are: A: alpine plateau climate, B: temperate continental climate, C: temperate monsoon climate, D: subtropical monsoon climate, E: tropical monsoon climate. Due to the small area of the E area and fewer weather stations, this study combines D and E areas into D for analysis.

Table 3 shows the trend and correlation of the annual ground surface freezing/thawing index with the annual mean ground surface temperature in different climatic regions. Although the correlations between the freezing thawing index and the surface temperature in the four sub-regions were slightly different, the correlation coefficients exceeded 0.9, in which the freezing/thawing index showed negative/positive correlations with the surface temperature, and the calculated results were all statistically significant. The thawing index of the D region changes most obviously with temperature, whereas that of the C region changes little with temperature. Similarly, by comparing the change in the freezing index in different regions, it can be found that the change in the freezing index in region C is the most obvious, whereas that in region D is the least.

Table 3. The variation trend of freezing/thawing index with temperature in different climatic regions in China from 1960 to 2020.

	Thawing Index		Freezing Index	
	Slope	R	Slope	R
A	478.84	0.93 **	−242.18	−0.90 **
B	431.14	0.96 **	−298.86	−0.93 **
C	357.89	0.94 **	−367.93	−0.95 **
D	645.62	0.99 **	−49.77	−0.91 **

Note: ** denotes significance at $p < 0.01$; A: alpine plateau climate; B: temperate continental climate; C: temperate monsoon climate; D: subtropical monsoon climate and tropical monsoon climate.

It can be seen from Figure 15 that the thawing index of the four sub-regions have similar trends under the five scenarios in the future. In the first and second warming scenarios, the increase in the thawing index was small. In the third, fourth, and fifth warming scenarios, the thawing index showed a trend of significant increase, which was consistent with the trend of the whole region. Among them, the change of the five scenarios in region C is smaller than that in other regions, and the range of the five scenarios is 5100 °C-days to 6300 °C-days by 2100. The change of the five scenarios in region D is the largest, and the range of the five scenarios is 7400 °C-days to 9600 °C-days by 2100.

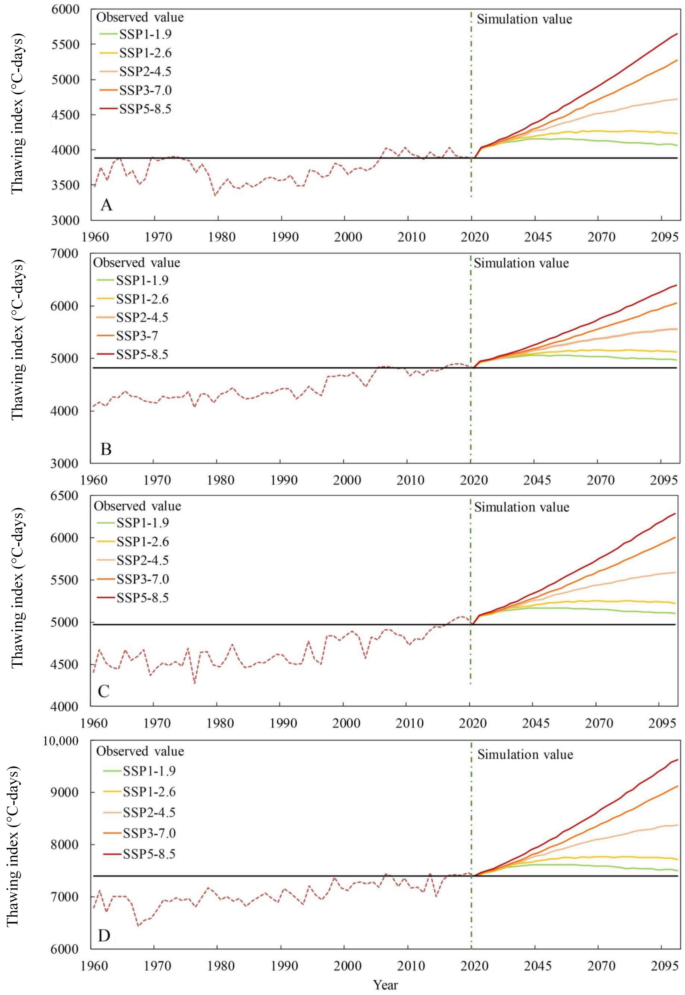


Figure 15. Variation of the thawing index in the four sub-regions in China, the red line is the observed thawing index from 1960 to 2020, whereas the black line is the observed thawing index in 2020 (**A**: alpine plateau climate; **B**: temperate continental climate; **C**: temperate monsoon climate; **D**: subtropical monsoon climate and tropical monsoon climate).

As can be seen from Figure 16, the trend of the freezing index in the four sub-regions is relatively consistent. In the first and second warming scenarios, the freezing index decreased gradually; after the middle of the 21st century, the freezing index increased. In the third, fourth, and fifth warming scenarios, the freezing index always presents a downward trend. In the fifth warming scenario, the freezing index of the four regions may be 0 in 2068, 2075, 2052, and 2032, respectively. By comparing the speed of the freezing index tending to 0 °C-days in different regions, it can be found that the freezing index tending to 0 °C-days in region B is the slowest in the five scenarios, whereas region D is the fastest.

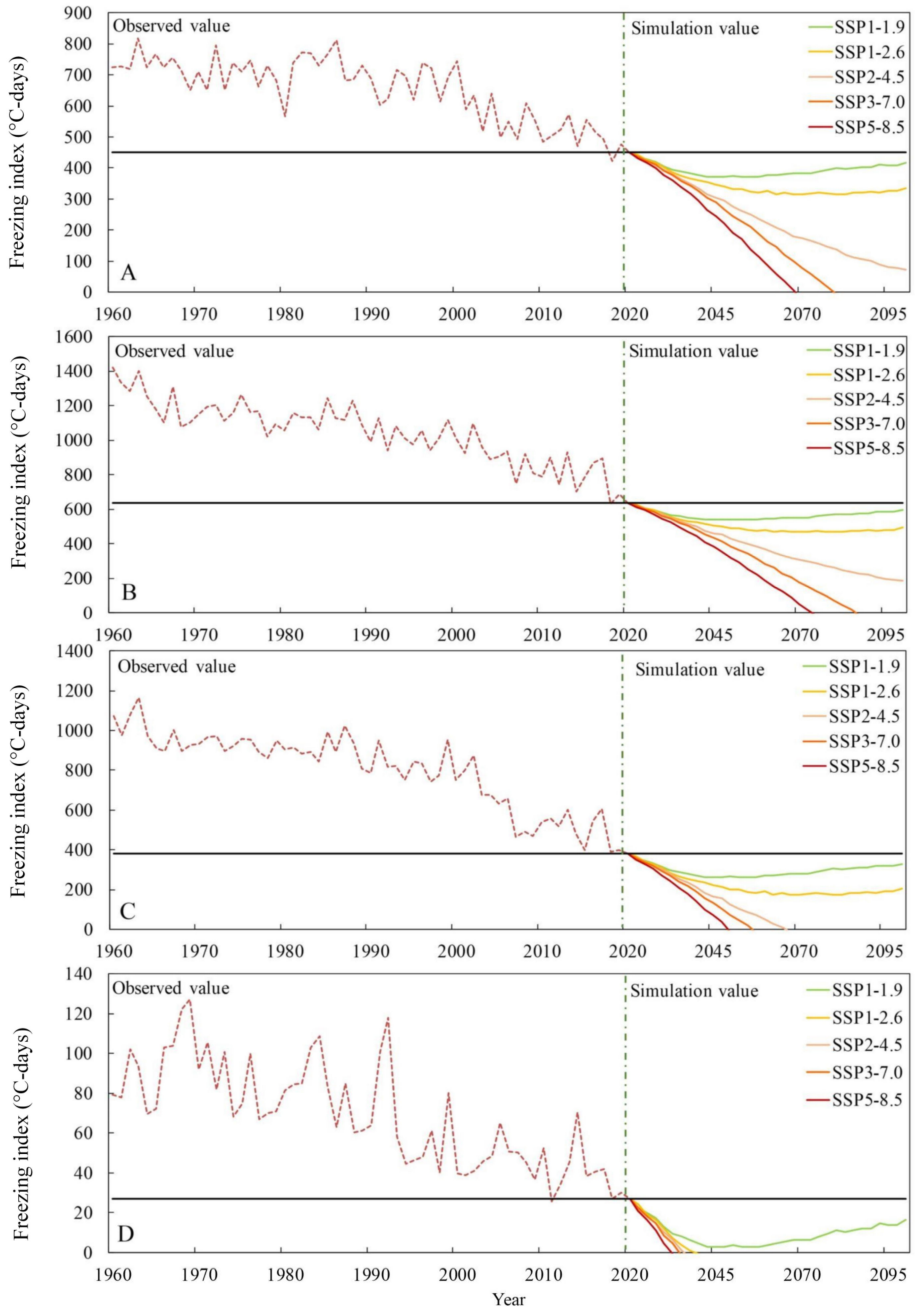


Figure 16. Variation of the freezing index in the four sub-areas in China, the red line is the observed freezing index from 1960 to 2020, whereas the black line is the observed freezing index in 2020 (**A**: alpine plateau climate; **B**: temperate continental climate; **C**: temperate monsoon climate; **D**: subtropical monsoon climate and tropical monsoon climate).

5. Conclusions

In this study, the annual ground surface freezing/thawing index was calculated based on the surface temperature data from meteorological stations from 1960 to 2020, and the time series of freezing/thawing indexes were statistically analyzed. In addition, the freezing/thawing index changes during the period of 2020–2100 were simulated by different warming scenarios of CMIP6. The following conclusions are drawn in accordance with the experimental results described above.

From 1960 to 2020, the thawing index shows an upward trend with increasing years, whereas the freezing index shows a downward trend with increasing years. After the mutation year, the thawing index and the freezing index show a stronger trend.

The results of the R/S analysis method show that the freezing index will maintain a downward trend in the future, whereas the thawing index will maintain an upward trend in the future (with strong inverse persistence and persistence), which coincides with the changing characteristics of the global climate.

The spatial–temporal variation characteristics of the freezing/thawing index during 2020–2100 were simulated. It is important to note that under the fifth warming scenario, the average thawing index in China will reach 7700 °C-days by 2100, and the average freezing index in China will reach 0 °C-days by 2070.

Author Contributions: X.L. and Z.Z. designed the paper. X.L. conducted the data processing, statistical analysis, and wrote the paper. A.M., M.Z., D.J. and J.Z. contributed great efforts to the research methodology, substantial editing, and figure optimization. All the authors contributed to the paper revision. All authors have read and agreed to the published version of the manuscript.

Funding: The authors greatly appreciate the support by the following research grants: (a) the National Natural Science Foundation of China (NSFC) (42011530083, 41825015, 42011530087); (b) Science & Technology Fundamental Resources Investigation Program (grant no. 2022FY100702); (c) the CAS "Light of West China" Program for the Belt and Road Research Teams (granted to Dr. Mingyi Zhang); (d) the Fundamental Research Funds for the Central Universities (2572022AW58).

Institutional Review Board Statement: Not applicable.

Informed Consent Statement: Not applicable.

Data Availability Statement: Published interpolated data sets are available from CMA (http://data.cma.cn/dataService/cdcindex/datacode/A.0013.0001/show_value/normal.html (accessed on 18 July 2021)). All warming scenarios data are available from CMIP6 (https://esgf-node.llnl.gov/search/cmip6/ (accessed on 18 July 2021)). Permafrost type data are available from (http://nsidc.org/data/ (accessed on 18 July 2021)).

Acknowledgments: The authors would like to thank the China Meteorological Administration (CMA), Coupled Model Intercomparison Project phase 6 (CMIP6), and National Snow and Ice Data Center/World Data Center (NSIDC) for providing the study data.

Conflicts of Interest: The authors declare no conflict of interest.

References

1. Guo, D.; Wang, H.; Li, D. A projection of permafrost degradation on the Tibetan Plateau during the 21st century. *J. Geophys. Res. Atmos.* **2012**, *117*, D5. [CrossRef]
2. Tett, S.F.; Stott, P.A.; Allen, M.R.; Ingram, W.J.; Mitchell, J.F. Causes of twentieth-century temperature change near the Earth's surface. *Nature* **1999**, *399*, 569–572. [CrossRef]
3. Gu, Y.; Lin, J.; Wang, X.L.; Zhang, X.J. Trend of annual runoff for major rivers in China under climate Change. *Procedia Eng.* **2012**, *28*, 564–568. [CrossRef]
4. Kolanowska, M.; Michalska, E.; Konowalik, K. The impact of global warming on the niches and pollinator availability of sexually deceptive orchid with a single pollen vector. *Sci. Total Environ.* **2021**, *795*, 148850. [CrossRef] [PubMed]
5. Wang, S.; Jin, H.; Li, S.; Zhao, L. Permafrost degradation on the Qinghai–Tibet Plateau and its environmental impacts. *Permafr. Periglac. Process.* **2000**, *11*, 43–53. [CrossRef]
6. Jorgenson, M.T.; Racine, C.H.; Walters, J.C.; Osterkamp, T.E. Permafrost degradation and ecological changes associated with a warming climate in central Alaska. *Clim. Change* **2001**, *48*, 551–579. [CrossRef]

7. Guglielmin, M.; Evans, C.J.; Cannone, N. Active layer thermal regime under different vegetation conditions in permafrost areas. a case study at Signy Island (Maritime Antarctica). *Geoderma* **2008**, *144*, 73–85. [CrossRef]
8. Koven, C.D.; Ringeval, B.; Friedlingstein, P.; Ciais, P.; Cadule, P.; Khvorostyanov, D.; Krinner, G.; Tarnocai, C. Permafrost carbon-climate feedbacks accelerate global warming. *Proc. Natl. Acad. Sci. USA* **2011**, *108*, 14769–14774. [CrossRef]
9. Volokhov, S.S. Effect of freezing conditions on the shear strength of soils frozen together with materials. *Soil Mech. Found. Eng.* **2003**, *40*, 233–238. [CrossRef]
10. Qi, J.; Yao, X.; Yu, F.; Liu, Y. Study on thaw consolidation of permafrost under roadway embankment. *Cold Reg. Sci. Technol.* **2012**, *81*, 48–54. [CrossRef]
11. Wen, Z.; Yu, Q.; Ma, W.; Dong, S.; Wang, D.; Niu, F.; Zhang, M. Experimental investigation on the effect of fiberglass reinforced plastic cover on adfreeze bond strength. *Cold Reg. Sci. Technol.* **2016**, *131*, 108–115. [CrossRef]
12. Chai, M.; Mu, Y.; Zhang, J.; Ma, W.; Liu, G.; Chen, J. Characteristics of asphalt pavement damage in degrading permafrost regions: Case study of the Qinghai–Tibet highway, China. *J. Cold Reg. Eng.* **2018**, *32*, 05018003. [CrossRef]
13. Cheng, G.; Zhao, L.; Li, R.; Wu, X.; Sheng, Y.; Hu, G.; Zou, D.; Jin, H.; Li, X.; Wu, Q. Characteristic, changes and impacts of permafrost on Qinghai-Tibet Plateau. *Chin. Sci. Bull.* **2019**, *64*, 2783–2795. [CrossRef]
14. Shi, Y.; Niu, F.; Lin, Z.; Luo, J. Freezing/thawing index variations over the circum-Arctic from 1901 to 2015 and the permafrost extent. *Sci. Total Environ.* **2019**, *660*, 1294–1305. [CrossRef]
15. Frauenfeld, O.W.; Zhang, T.; Mccreight, J.L. Northern hemisphere freezing/thawing index variations over the twentieth century. *Int. J. Climatol.* **2007**, *27*, 47–63. [CrossRef]
16. Nelson, F.; Outcalt, S. A computational method for prediction and regionalization of permafrost. *Arct. Alp. Res.* **1987**, *19*, 279–288. [CrossRef]
17. Zhang, T.; Frauenfeld, O.W.; Serreze, M.C.; Etringer, A.; Oelke, C.; McCreight, J.; Barry, R.G.; Gilichinsky, D.; Yang, D.; Ye, H.; et al. Spatial and temporal variability in active layer thickness over the Russian Arctic drainage basin. *J. Geophys. Res. Atmos.* **2005**, *110*, D16. [CrossRef]
18. Nelson, F.E.; Shiklomanov, N.I.; Mueller, G.R.; Hinkel, K.M.; Walker, D.A.; Bockheim, J.G. Estimating active-layer thickness over a large region: Kuparuk River basin, Alaska, USA. *Arct. Alp. Res.* **1997**, *29*, 367–378. [CrossRef]
19. Klene, A.E.; Nelson, F.E.; Shiklomanov, N.I. The n-factor as a tool in geocryological mapping: Seasonal thaw in the Kuparuk River Basin, Alaska. *Phys. Geogr.* **2001**, *22*, 449–466. [CrossRef]
20. Peng, X.; Zhang, T.; Cao, B.; Wang, Q.; Wang, K.; Shao, W.; Guo, H. Changes in freezing-thawing index and soil freeze depth over the Heihe River Basin, western China. *Arct. Antarct. Alp. Res.* **2016**, *48*, 161–176. [CrossRef]
21. Cheng, G.; Wu, T. Responses of permafrost to climate change and their environmental significance, Qinghai-Tibet Plateau. *J. Geophys. Res. Earth Surf.* **2007**, *112*, F2. [CrossRef]
22. Wu, Q.; Zhang, T. Changes in active layer thickness over the Qinghai-Tibetan Plateau from 1995 to 2007. *J. Geophys. Res. Atmos.* **2010**, *115*. [CrossRef]
23. Cao, B.; Zhang, T.J.; Peng, X.Q.; Zheng, L.; Mou, C.C.; Wang, Q.F. Analysis of the annual freeze-thaw index and its temporal and spatial changes in the Heihe River Basin. *Adv. Earth Sci.* **2015**, *30*, 357–366. (In Chinese)
24. Liu, X.; Li, J. Research on the spatiotemporal changes of freeze-thaw index in Northeast China from 1960 to 2012. *Heilongjiang Sci.* **2018**, *9*, 162–164. (In Chinese)
25. He, B.B.; Sheng, Y.; Huang, L.; Huang, X.B.; Zhang, X.Y. The change trend of freeze-thaw index in northern Xinjiang from 1961 to 2017. *J. Glaciol. Geocryol.* **2019**, *41*, 1107–1114. (In Chinese)
26. Jiang, F.; Hu, R.; Li, Z. Variations and trends of the freezing/thawing index along the Qinghai-Xizang Railway for 1966–2004. *J. Geogr. Sci.* **2008**, *18*, 3–16. [CrossRef]
27. Liao, Y.; Fan, H.; Li, Y.Y.; Cheng, G.W. Temporal and spatial changes of the freezing/thawing index of the Tibet Plateau from 1978 to 2017. *Pratacult. Sci.* **2021**, *38*, 1035–1046. (In Chinese)
28. Peng, X.; Zhang, T.; Liu, Y.; Luo, J. Past and projected freezing/thawing indices in the northern hemisphere. *J. Appl. Meteorol. Climatol.* **2019**, *58*, 495–510. [CrossRef]
29. Solang, T.J.; Du, J.; Tsewang, D.Z.; Phuntsok, S.D. Characteristics of annual freeze-thaw index in Qiangtang Nature Reserve under the background of climate warming. *Highl. Mt. Meteorol. Res.* **2021**, *41*, 48–55. (In Chinese)
30. Jian, B.; Li, J.; Zhao, Y.; He, Y.; Wang, J.; Huang, J. Evaluation of the CMIP6 planetary albedo climatology using satellite observations. *Clim. Dyn.* **2020**, *54*, 5145–5161. [CrossRef]
31. Wang, K.; Zhang, T.; Zhong, X. Changes in the timing and duration of the near-surface soil freeze/thaw status from 1956 to 2006 across China. *Cryosphere* **2015**, *9*, 1321–1331. [CrossRef]
32. Peng, X.; Zhang, T.; Frauenfeld, O.W.; Wang, K.; Cao, B.; Zhong, X.; Su, H.; Mu, C. Response of seasonal soil freeze depth to climate change across China. *Cryosphere* **2017**, *11*, 1059–1073. [CrossRef]
33. Wang, R.; Zhu, Q.; Ma, H. Changes in freezing/thawing index over the source region of the Yellow River from 1980 to 2014. *J. For. Res.* **2019**, *30*, 257–268. [CrossRef]
34. Wu, T.; Wang, Q.; Zhao, L.; Batkhishig, O.; Watanabe, M. Observed trends in surface freezing/thawing index over the period 1987–2005 in Mongolia. *Cold Reg. Sci. Technol.* **2011**, *69*, 105–111. [CrossRef]
35. Liu, W.; Xiong, H.; Liu, L.; Zhu, S.N.; Chen, X. Future climate change scenarios in the Ganjiang River Basin based on CMIP5 model and SDSM. *Res. Soil Water Conserv.* **2019**, *2*, 145–152. (In Chinese)

36. Jiang, D.; Hu, D.; Tian, Z.; Lang, X. Differences between CMIP6 and CMIP5 models in simulating climate over China and the East Asian monsoon. *Adv. Atmos. Sci.* **2020**, *37*, 1102–1118. [CrossRef]
37. Luo, N.; Guo, Y.; Gao, Z.; Chen, K.; Chou, J. Assessment of CMIP6 and CMIP5 model performance for extreme temperature in China. *Atmos. Ocean. Sci. Lett.* **2020**, *13*, 589–597. [CrossRef]
38. Li, C.; Jiang, T.; Wang, Y.; Miao, L.J.; Li, S.Y.; Chen, Z.Y.; Lv, Y.R. Modeled prediction of future temperature in the upper Yellow River based on CMIP6 model. *J. Glaciol. Geocryol.* **2022**, *44*, 171–178. (In Chinese)
39. Wu, T.; Lu, Y.; Fang, Y.; Xin, X.; Li, L.; Li, W.; Jie, W.; Zhang, J.; Liu, Y.; Zhang, L.; et al. The Beijing Climate Center climate system model (BCC-CSM): The main progress from CMIP5 to CMIP6. *Geosci. Model Dev.* **2019**, *12*, 1573–1600. [CrossRef]
40. Zhang, H.; Zhang, M.; Jin, J.; Fei, K.; Ji, D.; Wu, C.; Zhu, J.; He, J.; Chai, Z.; Xie, J.; et al. Description and Climate Simulation Performance of CAS-ESM Version 2. *J. Adv. Model. Earth Syst.* **2020**, *12*, e2020MS002210. [CrossRef]
41. Lauritzen, P.H.; Nair, R.D.; Herrington, A.R.; Callaghan, P.; Goldhaber, S.; Dennis, J.M.; Bacmeister, J.T.; Eaton, B.E.; Zarzycki, C.M.; Taylor, M.A.; et al. NCAR release of CAM-SE in CESM2. 0: A reformulation of the spectral element dynamical core in dry-mass vertical coordinates with comprehensive treatment of condensates and energy. *J. Adv. Model. Earth Syst.* **2018**, *10*, 1537–1570. [CrossRef]
42. Liu, S.M.; Chen, Y.H.; Rao, J.; Cao, C.; Li, S.Y.; Ma, M.H.; Wang, Y.B. Parallel comparison of major sudden stratospheric warming events in CESM1-WACCM and CESM2-WACCM. *Atmosphere* **2019**, *10*, 679. [CrossRef]
43. Golaz, J.C.; Caldwell, P.M.; Van Roekel, L.P.; Petersen, M.R.; Tang, Q.; Wolfe, J.D.; Abeshu, G.; Anantharaj, V.; Asay-Davis, X.S.; Bader, D.C.; et al. The DOE E3SM coupled model version 1: Overview and evaluation at standard resolution. *J. Adv. Model. Earth Syst.* **2019**, *11*, 2089–2129. [CrossRef]
44. Yukimoto, S.; Kawai, H.; Koshiro, T.; Oshima, N.; Yoshida, K.; Urakawa, S.; Tsujino, H.; Deushi, M.; Tanaka, T.; Hosaka, M.; et al. The Meteorological Research Institute Earth System Model version 2.0, MRI-ESM2. 0: Description and basic evaluation of the physical component. *J. Meteorol. Soc. Jpn.* **2019**, *97*, 931–965. [CrossRef]
45. Partal, T.; Kahya, E. Trend analysis in Turkish precipitation data. *Hydrol. Process. Int. J.* **2006**, *20*, 2011–2026. [CrossRef]
46. Ramachandra, R.A.; Azli, M.; Pae, L.J. Identification of trends in Malaysian monthly runoff under the scaling hypothesis. *Hydrolog. Sci. J.* **2011**, *56*, 917–929. [CrossRef]
47. Di Giuseppe, E.; Pasqui, M.; Magno, R.; Quaresima, S. A Counting Process Approach for Trend Assessment of Drought Condition. *Hydrology* **2019**, *6*, 84. [CrossRef]
48. Men, B.; Liu, C.; Xia, J.; Liu, S.X.; Lin, Z.H. Application of R/S Analysis Method in the Prediction of Runoff Trend of Water Diversion Rivers in the West Route of the South-to-North Water Diversion Project. *J. Glaciol. Geocryol.* **2005**, *4*, 568–573. (In Chinese)
49. Zhang, X.; Cai, H.; Yin, X. Application of Rescaled Range Analysis (R/S) to analyze water and sediment changes in Wuding River Basin. *Trans. Chin. Soc. Agric. Eng.* **2010**, *26*, 212–217. (In Chinese)
50. Zhang, J.; Hu, Q.; Wang, S.; Ai, M. Variation Trend Analysis of Runoff and Sediment Time Series Based on the *R/S* Analysis of Simulated Loess Tilled Slopes in the Loess Plateau, China. *Sustainability* **2018**, *10*, 32. [CrossRef]
51. Mandelbrot, B.B.; Wallis, J.R. Some Log-Run Properties of Geophysical Records. *Water Resour. Res.* **1969**, *5*, 321–340. [CrossRef]
52. Mandelbrot, B.B.; Wallis, J.R. Robustness of the rescaled range R/S in the measurement of noncyclic long run statistical dependence. *Water Resour. Res.* **1969**, *5*, 967–988. [CrossRef]
53. Li, X.; Jin, H.; Sun, L.; Wang, H.; He, R.; Huang, Y.; Chang, X. Climate warming over 1961–2019 and impacts on permafrost zonation in Northeast China. *J. For. Res.* **2021**, *33*, 767–788. [CrossRef]